Hindawi
International Journal of Rotating Machinery
Volume 2022, Article ID 5994933, 13 pages
https://doi.org/10.1155/2022/5994933

Research Article

Effects of Diffusion Film Hole Exit Area on the Film Cooling Effectiveness

Fan Yang and Mohammad E. Taslim

Mechanical and Industrial Engineering Department, Northeastern University, Boston, Massachusetts 02115, USA

Correspondence should be addressed to Mohammad E. Taslim; m.taslim@neu.edu

Received 17 July 2022; Revised 29 August 2022; Accepted 1 September 2022; Published 17 September 2022

Academic Editor: Kenneth Van Treuren

One popular method for the protection of gas turbines' hot sections from high-temperature combustor gases is film cooling. Substantial amounts of research have been conducted to accomplish this task with the minimum cooling flow, maximum surface coverage, and minimal aerodynamic inefficiencies or structural penalties. In this study, a combined experimental and numerical investigation was conducted on three selected film-cooling hole geometries. These geometries were designed with the same initial metering (feed) section, a cylindrical hole of 30° inclination angle, followed by three different forward expansion section geometries. The expansion sections had a 7° laid-back angle and a 17° expansion angle in each lateral direction. However, different interior corner radii were used to blend the metering hole to the exit area, creating three different expansion geometries with almost the same exit areas. In practice, this variation in expansion geometry could represent manufacturing faults or tolerances in laser drilling of the film holes. This study shows that the variations in film-cooling effectiveness are not significant even though the expansion geometries are significantly different. The Pressure Sensitive Paint (PSP) technique was used to obtain the detailed distribution of film-cooling effectiveness on the surface area downstream of these film holes. Adiabatic film cooling effectiveness was measured at blowing ratios of 0.5, 1.0, and 2.0. CFD models of these film holes were also run, and the results were compared with the test data. The major conclusions of this study were that these proposed new geometries produced higher film effectiveness than the conventional 7°-7°-7° diffusion film holes, for the same exit area, the expansion section geometry of the film holes did not have a significant effect on the film coverage, and the numerical results were in good agreement with the test data.

1. Introduction

With the increasing demand for propulsion power and higher cycle thermal efficiencies, higher turbine inlet temperatures and higher compressor pressure ratios are required for modern gas turbines [1]. In some industrial applications, the temperature of the exhaust gases from the combustion chamber can reach as high as 1000-1400 K [2, 3] while in some advanced military engines, that temperature can reach 1800 K [4, 5]. However, the materials of the hot section parts of the modern gas turbines cannot survive the extreme temperatures and loads. Therefore, both internal and external cooling methods are needed to protect the components from failure.

The film cooling technique is an effective approach to protect the advanced gas turbine airfoils [6–8]. In this process, cooling gas passes through the internal cooling channels and emerges from the film holes to create a blanket of thin film over the outer surface of the airfoil thus preventing the direct contact of the hot gases and the coverage surfaces. The overall film cooling performance is affected by both flow conditions and hole geometry. Increasing the cooling performance at the expense of small aerodynamic losses is the goal in all designs. Early researchers [9, 10] have found theoretically that an ideal tangential-shaped slot can lead to a continuous and uniform film layer. For discrete film holes, however, the interaction between the injected coolant and hot main flow can lead to a complex flow structure. The cooling performance of the basic shapes of film holes can be found in the review by Goldstein [10]. The overall performance is affected by various parameters: hot/cooling flow conditions, cooling hole

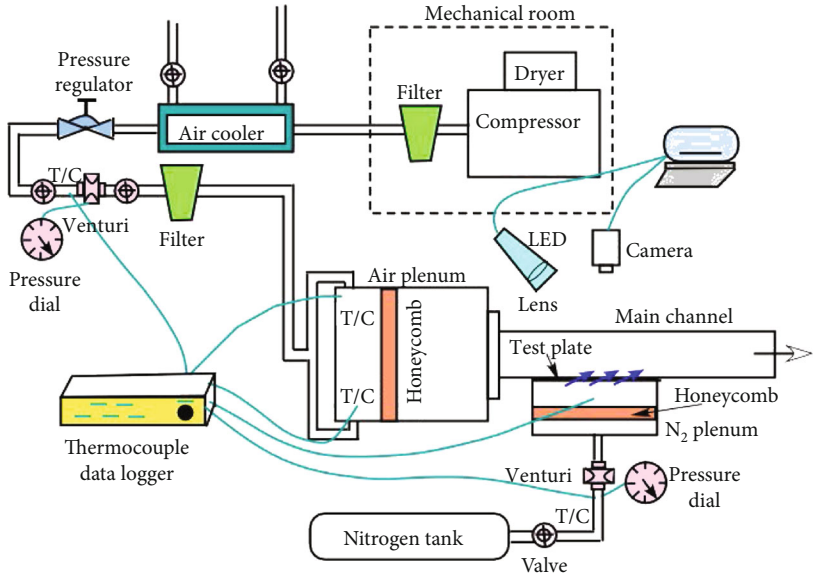

Figure 1: Test rig, associated accessories, and data collection equipment.

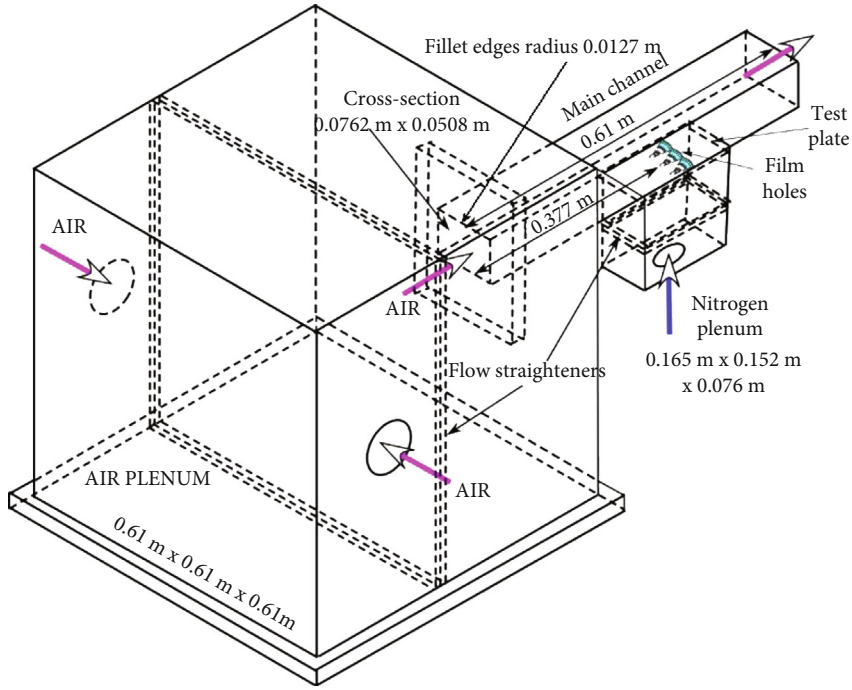

Figure 2: Schematics of the test rig.

geometry, surface roughness, etc. [11]. As for the film hole geometry, inclination angle, compound angle, hole pitch, and hole arrangements are the main parameters that affect the film cooling effectiveness. Compared to straight cylindrical holes, fan-shaped holes with diffusion exits can create a more uniform distribution of coolant on the lateral surface. However, as the diffusion increases, the aerodynamic losses also increase. For example, the research of Day et al. [12] showed that the aerodynamics loss of a cascade with fan-shaped holes was increased by 7.7 percent, compared with that of the cylindrical holes. Thus, over the years, researchers [13–23] have developed numerous shapes to improve the overall film cooling performance. Most of their studies were focused on shaped holes with different inclination angles, lateral/laidback expansion angles, and hole spacing.

In recent studies, researchers numerically and experimentally optimized the cooling hole geometry configuration. Schroeder and Thole [24] provided a baseline shaped cooling hole with a 30° inclination angle and 7° expansion in forward and lateral directions. This baseline shape has a typical hole length of 6 diameters and pitch of 6 diameters, which appeared regularly in literature. Based on the 7°-7°-7° baseline geometry, Haydt et al. [25] increased the expansion angle to 12° and tested the effect of the area ratio. In their study, a higher area

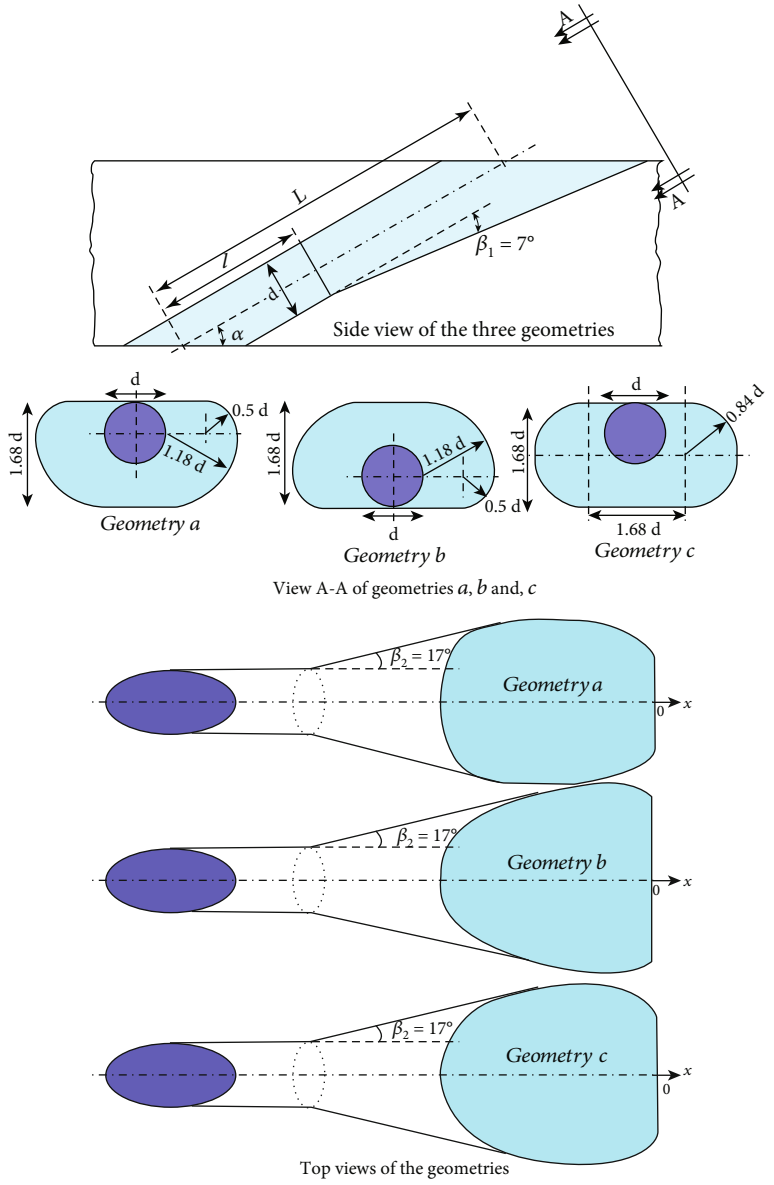

Figure 3: Details of the film hole geometries.

ratio can bring higher effectiveness, especially at high blowing ratios. However, at low blowing ratios, their 12°-12°-12° hole was taking hot flow ingestion because of the large opening. Also, the steady Reynolds-averaged Navier-Stokes simulations did not fully agree with the experimental results in their case. Sun et al. [26] also did a comparison between four common film holes with the same hole exit areas: cylindrical, fan-shaped, double jet, and the main hole with sister holes. In their study, the double jet hole had the best performance due to the complex flow structure created by the interaction between the coolant and the main flow. Hole geometry with sister holes also maintained a good film cooling effectiveness by inhibiting the kidney vortices. They also showed that, for their shaped hole and double jet holes, the numerical results using the realizable k-ε, RNG k-ε, and SST k-ω models were in less agreement with the experimental data, compared to the other two film-hole geometries. Watson et al. [27] compared their new oblong, racetrack-shaped inlet with the 12°-12°-12° laidback, fan-shaped hole inlet. Their film hole with an area ratio (exit to inlet) of 2 : 1 successfully reduced the negative effects of the secondary flows. Because of the increased film-hole exit area, their design with considerable diffusion performed better than the 12°-12°-12° geometry.

In the present study, the performance of three film-hole geometries with different diffusion section geometries but the same exit area values are compared. These holes have the same inclination angle, the same lateral/laidback expansion angle, the same hole spacing, and the same metering section. The only difference between them is the transition from the initial metering/feed hole to the exit opening area in the diffusion sections by varying the corner radii which could represent the manufacturing tolerances.

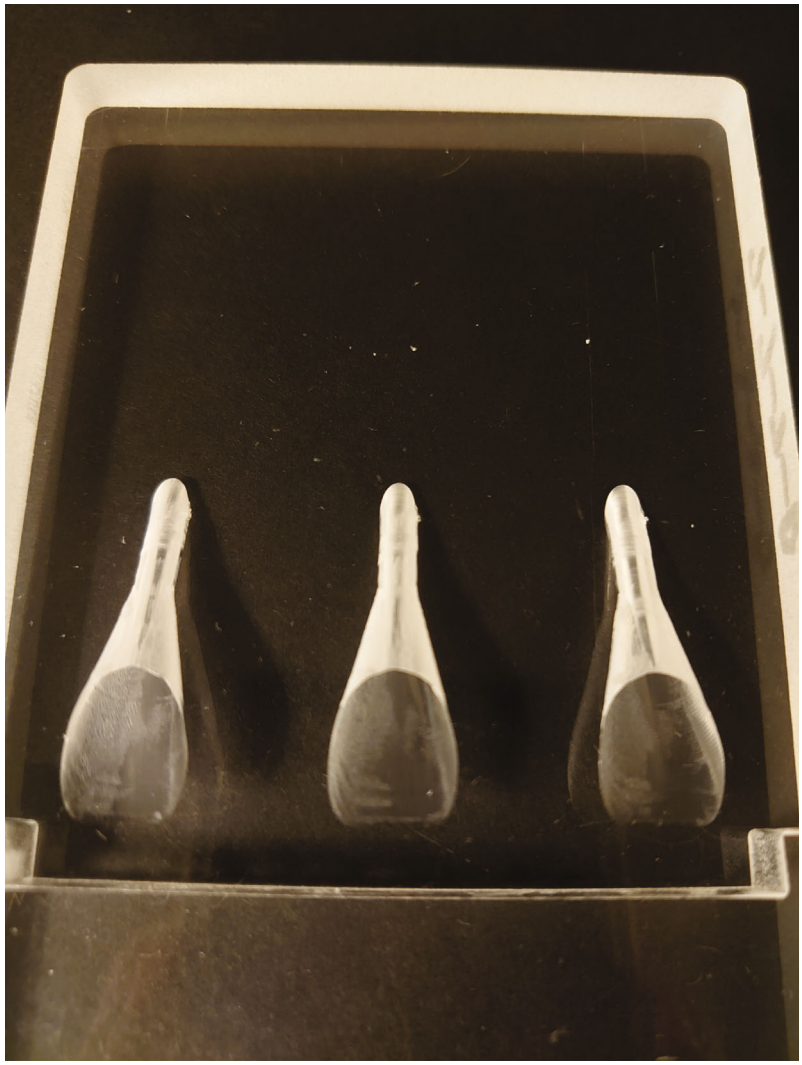

Figure 4: Machined *Geometry b* before testing.

2. Experimental Setup

The film cooling performance was investigated in an open-loop flow path as shown in Figure 1. A 100-psi air compressor was the source of the main flow. The air passed through a cooler and two filters before entering the air plenum. A honeycomb flow straightener was used to minimize the lateral velocity components of the main flow before entering the test channel. The Nitrogen gas, the coolant, was also passed through a separate plenum with a honeycomb flow-straightener before entering the film holes. Two critical venturis, chocked all the time, measured the main flow and coolant flow rates. The removable test plates, with three machined film holes for each geometry, were installed on the partition between the nitrogen plenum and the main flow channel flush with the main channel floor. A data acquisition system with k-type thermocouples, positioned at strategic points measured the air and nitrogen temperatures. An ultraviolet LED light of 400 nm wavelength passing through a double-convex lens was cast on the test plate. A CCD camera of 1600 × 1200 resolution and a 610 nm red filter recorded the illuminance intensity distribution. Details of the test rig are

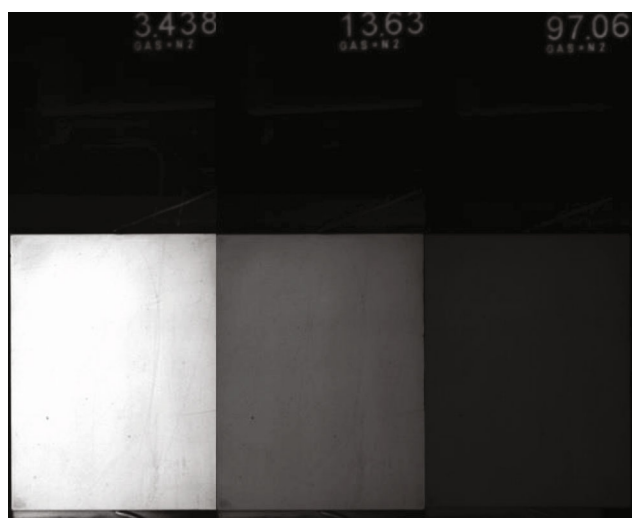

Figure 5: Black and white images of light intensity on the sprayed aluminum coupon in the calibration vacuum chamber.

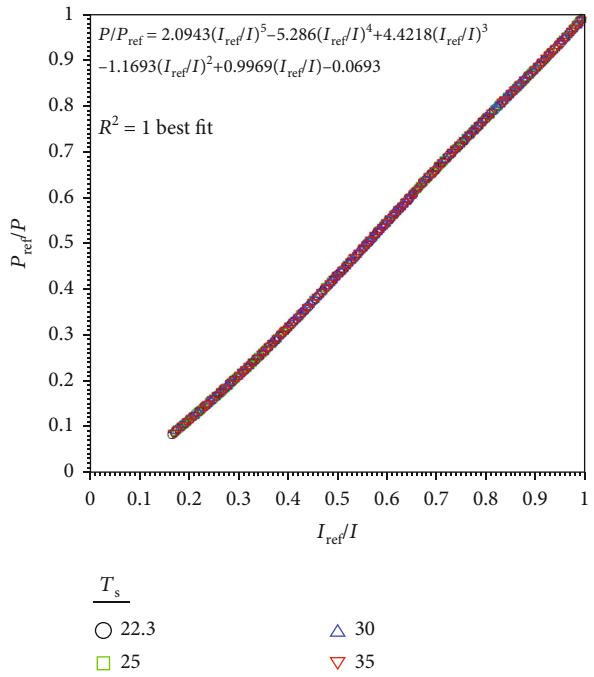

Figure 6: PSP calibration at different temperatures: 22.3, 25, 30, and 35°C.

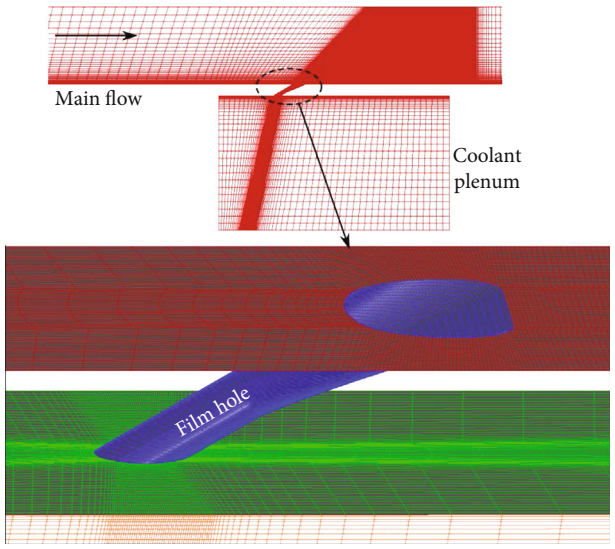

Figure 7: Computational model and mesh distribution around a typical film hole (*Geometry c*).

shown in Figure 2. The main flow channel as well as plenums was fabricated with clear acrylic plastic slabs. The test plates were also fabricated out of clear acrylic plastic slabs. The three hole geometries in this study are shown in Figure 3. All these holes have a 30° cylindrical metering section of 2.5 d length. The expansion section of these holes with expansion angles of 7°, 17°, and 17° create exit areas that differ by about ±3% on average. Film holes were machined on the test plate at a pitch-to-diameter ratio, p/d, of 6.0. Measurements were performed on the entire test section, but the reported data are for the middle hole to eliminate any edge effects. The exit areas have the same overall width and length as seen in Figure 3. However, the way the expansion sections are blended in with the metering holes causes a small difference in exit areas. A typical machined test plate of size 17.78 cm × 7.62 cm × 1.143 cm with three *Geometry b* film holes before the application of the pressure-sensitive paint is shown in Figure 4.

2.1. Pressure Sensitive Paint Methodology. Pressure-sensitive paint (PSP) technique is a popular method used by researchers to measure the adiabatic film cooling effectiveness distributions on the surfaces simulating the gas turbine hot sections in test setups during the past three decades. The similarity between the mass transfer on an impermeable wall and heat transfer on an adiabatic wall leads to the following equation for the film cooling effectiveness [28].

$$\eta = \frac{C_{aw} - C_\infty}{C_c - C_\infty} = 1 - \frac{1}{1 + \left(P_{O_2,air}/P_{O_2,mix} - 1\right)\left(M_{N_2}/M_{air}\right)}. \quad (1)$$

As early as 1990, Kavandi et al. [29] dissolved platinum octaethyl porphyrin ($C_{36}H_{46}N_4$) in a silicone matrix to form a thin film over their test surface. The proportionality between the luminescence intensity and oxygen partial pressure made it possible to measure the oxygen partial pressure change with a commercial frame buffer board. Their success was a precedent for the use of pressure-sensitive paint in film cooling studies. Over the years, the PSP technique has been continuously improved. Compared with the traditional thermocouple method, temperature-sensitive paint, and infrared thermography, the PSP techniques can provide a continuous mapping of the test surface with excellent accuracy and since the main flow, the coolant, and the test section are all at the same temperature, there are no heat losses during the tests. Details can be found in an excellent review by Gregory et al. [30].

The fundamental working principle of PSP is the oxygen quenching of the luminescence. An LED light with a particular wavelength is needed to activate the paint. As the oxygen partial pressure on the paint surface changes, the illuminance intensity will also change. Researchers usually use air as the main flow and another pure gas like nitrogen or carbon dioxide as the coolant to obtain the oxygen partial pressure distribution on the target area which leads to the determination of the film-cooling effectiveness using Equation (1) above. The relation between the illuminance intensity and oxygen partial pressure can be expressed in the following equation [28]:

$$IR = \frac{I_{ref} - I_{black}}{I - I_{black}} = f\left(\frac{P}{P_{ref}}\right) = f\left(P_{O_2}\right), \quad (2)$$

where *IR* is the ratio of reference light intensity to the measured intensity. When a test is conducted, the PSP is transitioned to an excited singlet energy state when exposed to a high-intensity LED with UV 400 nm wavelength. To maintain the ground state, it emits photons of longer wavelengths. However, when the paint interacts with oxygen molecules, it becomes nonradiative. In this study, UniFIB® pressure-sensitive paint

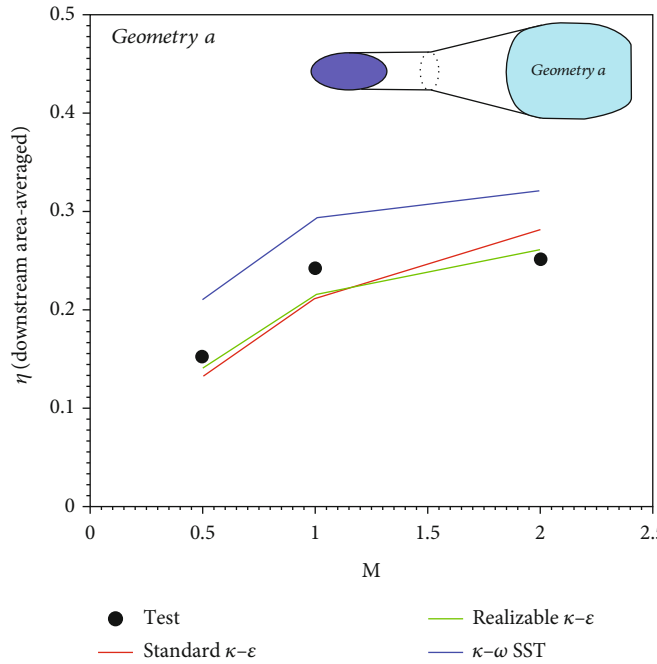

Figure 8: Comparison of different turbulence models with the test data for *Geometry a*.

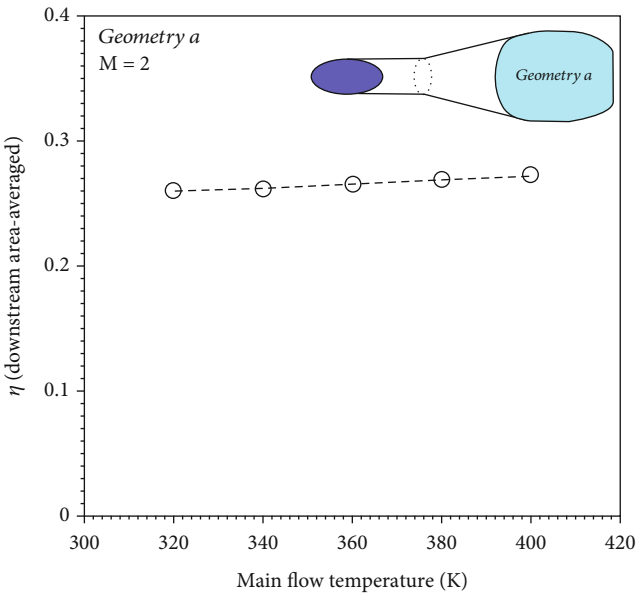

Figure 9: Temperature independence test for *Geometry a* at M = 2.0.

from ISSI Innovative Solutions Inc. was used. This paint showed a wide illuminance intensity range with high-pressure sensitivity and low-temperature sensitivity. A base coat was sprayed uniformly on all test plates with an air pump and a sprayer set. When the base coat was completely dried, the PSP was applied in the same manner. The paint was then cured in a lab oven at 70°C for two hours. Before performing the film effectiveness tests, the PSP had to be calibrated. The calibration test was performed using a painted aluminum plate placed in a sealed vacuum chamber. Details of the calibration procedure are given in Baldino and Taslim [31]. Figure 5 shows the black and white images of light intensity on the calibration aluminum coupon, spayed with the PSP, in the vacuum chamber. A 5th-degree polynomial shown in Figure 6 best represents the collected calibration data. This correlation between the illuminance intensity ratio and oxygen partial pressure ratio was used for data reduction in all film-cooling effectiveness measurements. All the photos were processed with ImageJ for the intensity data (grey value in this software) and MATLAB was used to transform the illuminance intensity to film-cooling effectiveness. The uncertainty analysis for the measured film effectiveness, based on the Kline and McClintock's method [32], was calculated to be ±5%, details of which are presented in Baldino and Taslim [31]. The main channel Reynolds number remained at a fixed value of 87200, corresponding to an air mass flow rate of 0.1016 kg/s in all tests. The coolant (nitrogen) mass flow rate, however, was varied depending on the desired blowing ratio of 0.5, 1 and 2. The freestream turbulence intensity in the main channel was measured to be 3.86%.

3. Numerical Study

The solid model for each geometry was created using the well-known Solidworks™ software. The main channel, the coolant plenum, and the three film hole geometries made up the computational domain. Each model was then imported to the ICEM-CFD™, a powerful meshing software by Ansys™. A typical computational domain and details of the mesh distribution around a typical film-hole geometry with two symmetric side walls are shown in Figure 7. In their entirety, the computational domains were meshed with hexahedral elements, a preferred choice for CFD analyses. Elements were varied in size bigeometrically from the boundaries to the core of the computational domain in order to have finer mesh close to the boundaries. Fluent/UNS by Ansys, Inc., a pressure-correction based,

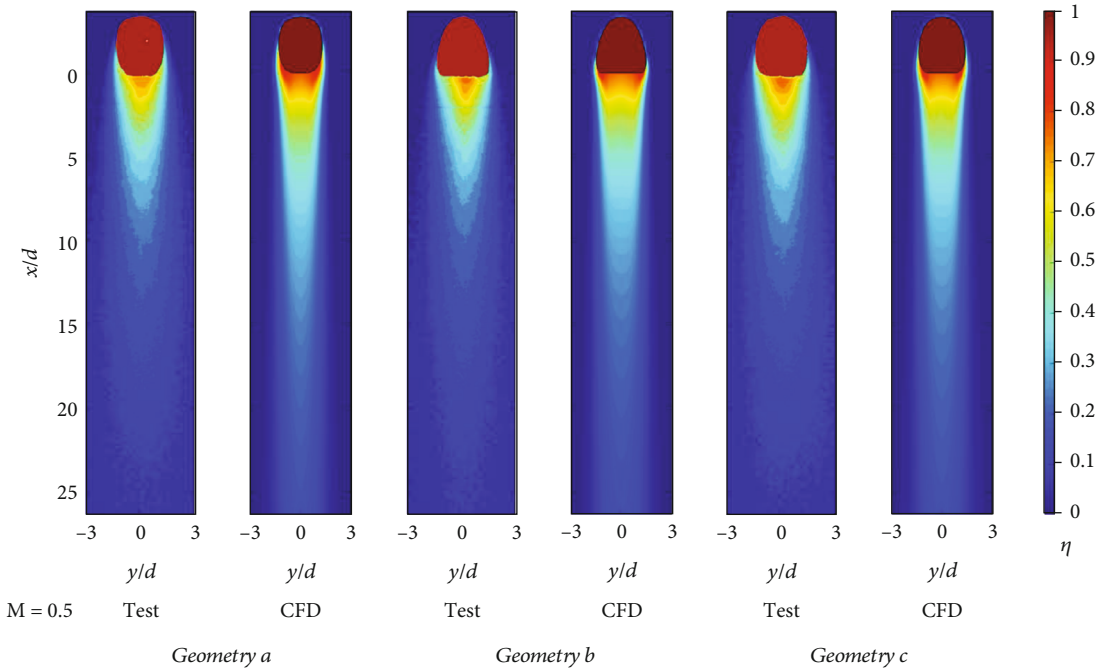

Figure 10: Test and CFD comparison of effectiveness contours for the blowing ratio of 0.5.

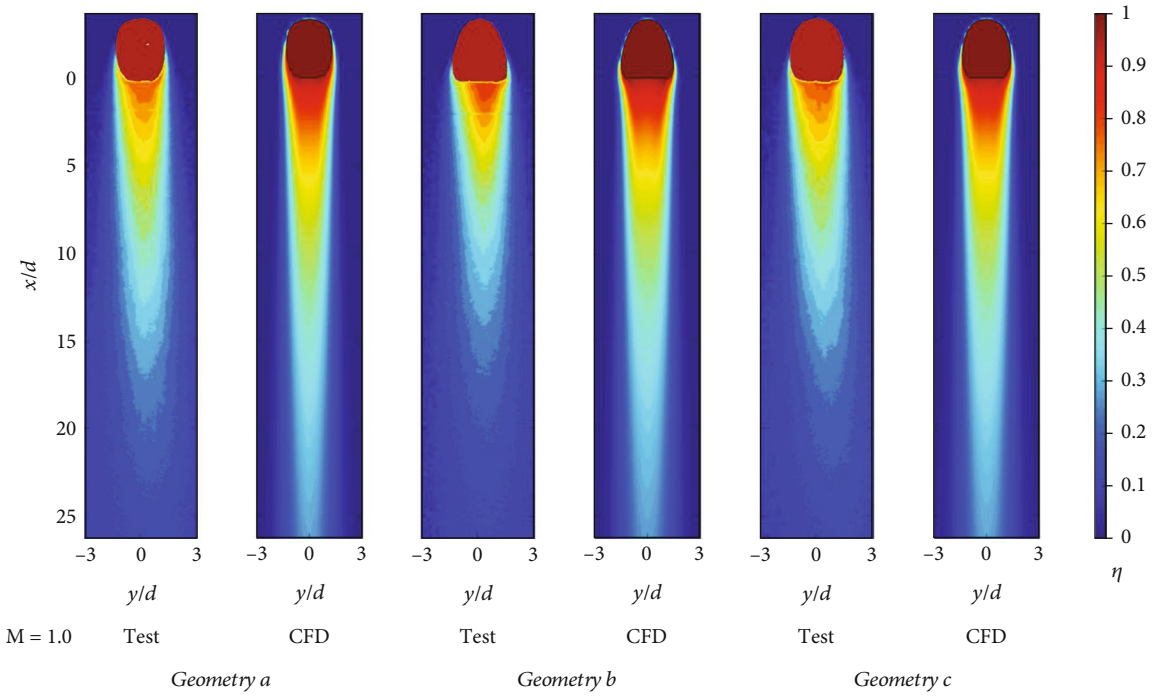

Figure 11: Test and CFD comparison of effectiveness contours for the blowing ratio of 1.

multiblock, multigrid, and unstructured/adaptive solver was used in this study. As for the turbulence model, the standard k-ε, realizable k-ε and k-ω SST models were tested for *Geometry a*, the results of which are compared with the test data in Figure 8. It was, therefore, concluded that the realizable k-ε model produced the closest results to the test data. Inlet boundary conditions for the main flow and coolant channels were identical to the test mass flow rates. Main flow and coolant temperatures were set to 320 K and 300 K, respectively, and adiabatic condition was set for all walls. Several numerical cases of *Geometry a* with the main flow temperatures ranging from 320 K to 400 K were run with no significant difference (<3%) in the resulting area-weighted average film effectiveness on the entire downstream area of the cooling hole. Results are

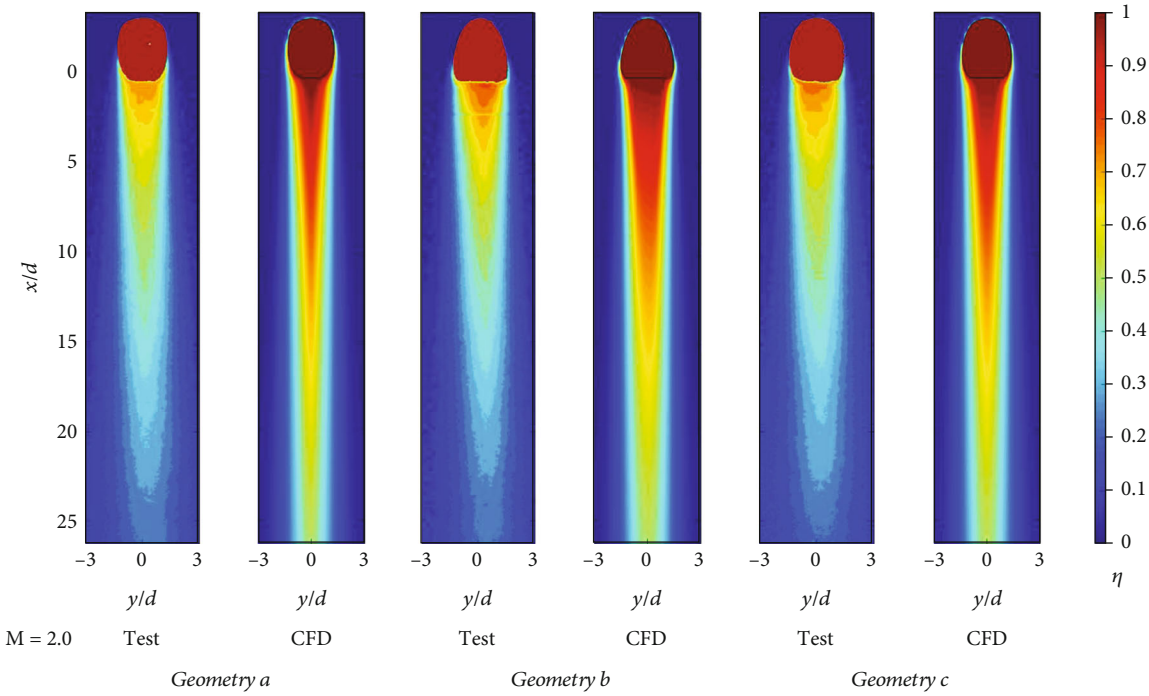

Figure 12: Test and CFD comparison of effectiveness contours for the blowing ratio of 2.

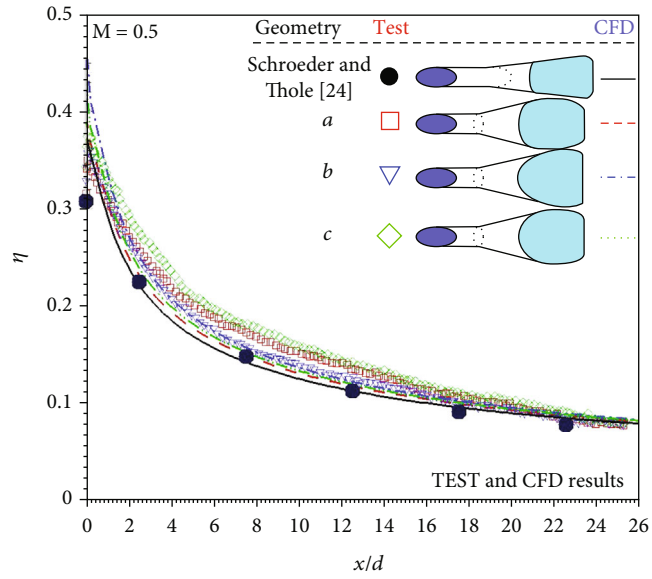

Figure 13: Laterally averaged film effectiveness for M = 0.5.

shown in Figure 9. Main channel exit condition was set to that of the lab pressure and the freestream turbulence intensity was set to the value measured in the test section (3.86%). Mesh independence was achieved at about 2.5 million elements thus all numerical models were run with 3 million hexahedral elements. Ideal gas law for density and Sutherland model for viscosity were activated. For convergence of numerical runs, the residual sums for all variables were set to less than 1×10^{-7} and that was accomplished at about 30,000 iterations.

4. Results and Discussion

Figures 10–12 represent the experimental as well as numerical film effectiveness distribution downstream the proposed film holes for the three blowing ratios of 0.5, 1, and 2. With the increase of the blowing ratio from Figures 10–12, the film coverage improves accordingly. This is a commonly observed performance for the laidback, fan-shaped film holes. Before we present the spanwise-averaged film effectiveness for the three

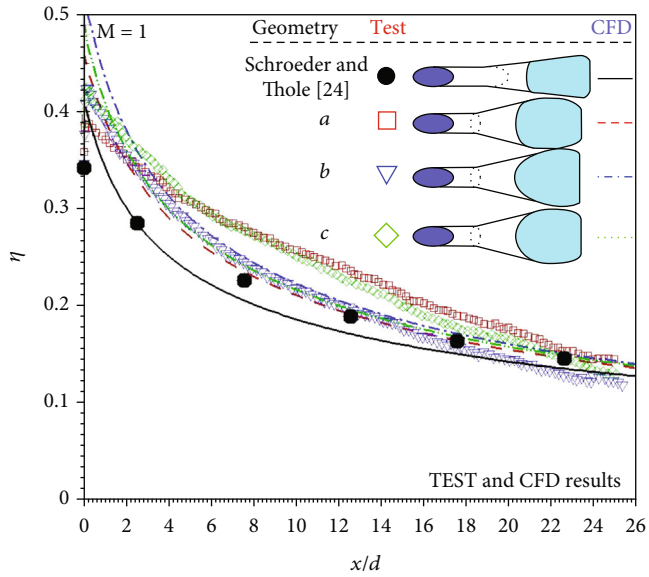

Figure 14: Laterally averaged film effectiveness for M = 1.

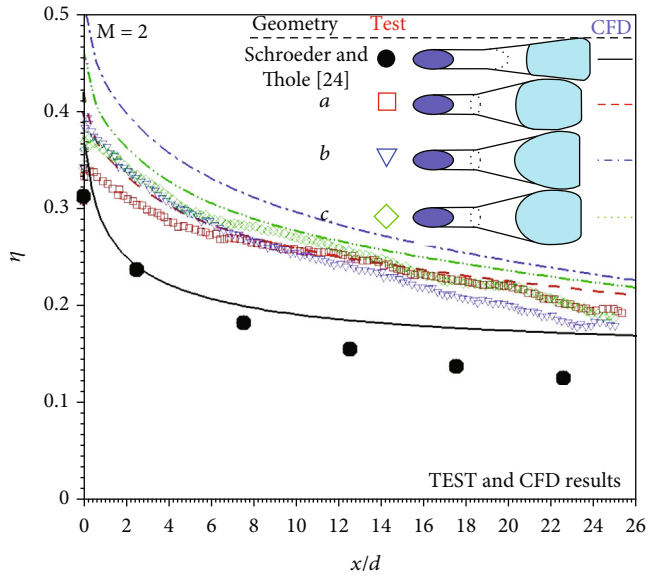

Figure 15: Laterally averaged film effectiveness for M = 2.

Table 1: Area-averaged effectiveness.

Effectiveness		Geometry		Geometry		Geometry	
η	M	a		b		c	
	0.5	0.1528		0.146		0.1614	
Experimental	1	0.2412		0.2155		0.2391	
	2	0.2517	%Diff.	0.2501	%Diff.	0.2615	%Diff.
	0.5	0.1412	-8.22%	0.1497	2.47%	0.1447	-11.54%
CFD	1	0.2152	-12.08%	0.2288	5.81%	0.2212	-8.09%
	2	0.261	3.56%	0.2972	15.85%	0.2783	6.04%

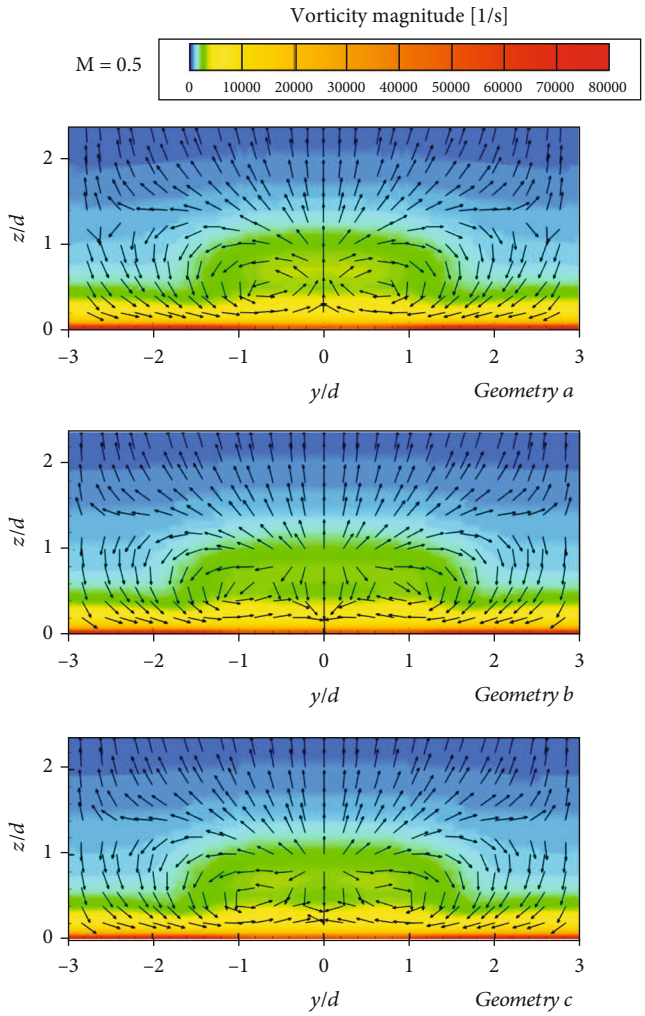

Figure 16: Vorticity magnitude contours and velocity vectors at x /d = 5, for the three film hole geometries, M = 0.5.

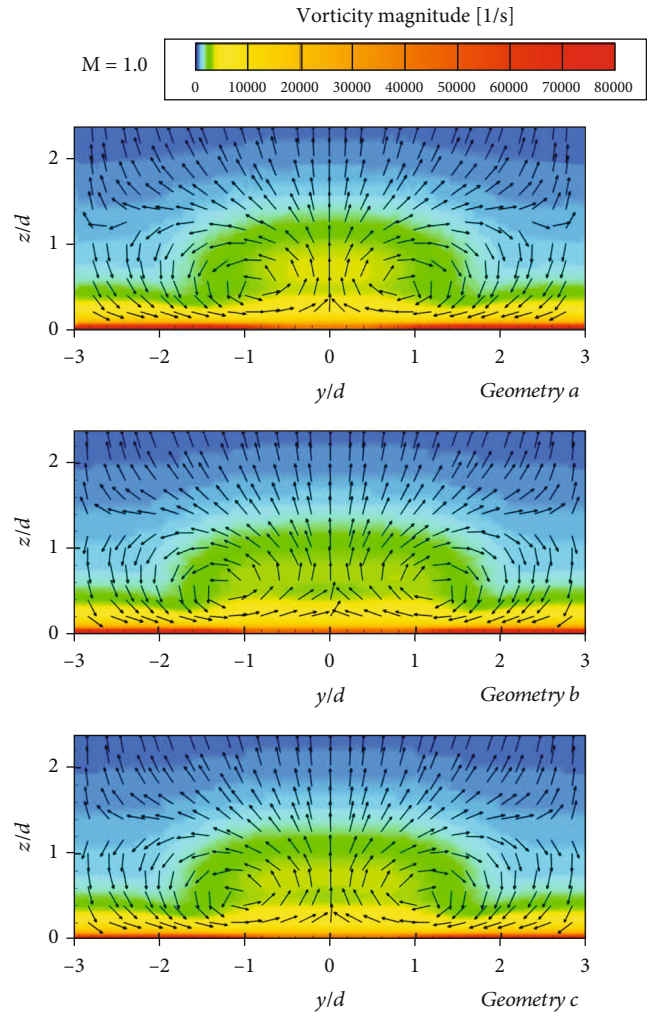

Figure 17: Vorticity magnitude contours and velocity vectors at x /d = 5, for the three film hole geometries, M = 1.

geometries and make a comparison, these contours do not show a significant difference in film coverage for the three film hole geometries. One observable difference is that the coverage area for *Geometry b* is a bit wider due to the wider straight edge of its exit area. Numerical film effectiveness distribution downstream of each film hole geometry is shown next to the experimental data for the three blowing ratios. The numerical results are generally in agreement with the experimental data. However, the penetration of coolant into the main flow, downstream the film holes exit, is longer in the numerical cases indicating the higher momentum of the coolant exiting the film holes. Machining tolerances around the exit area edges could be a reason for this difference.

Streamwise variations of the laterally averaged film effectiveness are presented in Figures 13–15. Each figure represents a blowing ratio. Other than our own proposed geometries, for comparisons, we have included the test data for the conventional popular 7°-7°-7° diffusion hole geometry reported by Schroeder and Thole [24]. The numerical results for the 7°-7°-7° diffusion hole geometry are from our simulations using the same setup. Several observations are made. First, our proposed film hole geometries performed better than the commonly used 7°-7°-7° diffusion hole geometry for all tested blowing ratios. It should be noted that our density ratio was close to unity while theirs was 1.2. However, other parameters were identical. Second, as expected for the diffusion holes, the film effectiveness increased with the blowing ratio. Third, the agreement between the test and numerical results, especially at lower blowing ratios, is very good. Fourth, the three different expansion section geometries of the film holes did not have a significant effect on the film coverage, in particular for the lower blowing ratios.

Table 1 lists the area-averaged film effectiveness for the three film hole geometries and the three blowing ratios. The area under consideration is from $(x/d, y/d) = (0, -3)$ to $(x/d, y/d) = (25, 3)$ in Figure 3. The percentage difference in the area-averaged film effectiveness values between the experimental and numerical results vary from a minimum of about 2.5% for the *Geometry b* at a blowing ration of 0.5 to a maximum of about 16% for the same geometry at a blowing ratio of 2. Given the experimental uncertainty of ±5%, most cases are in reasonable agreement. Higher values for the numerical cases are due to a longer penetration of the coolant into the main flow as is evidenced in Figures 10–12.

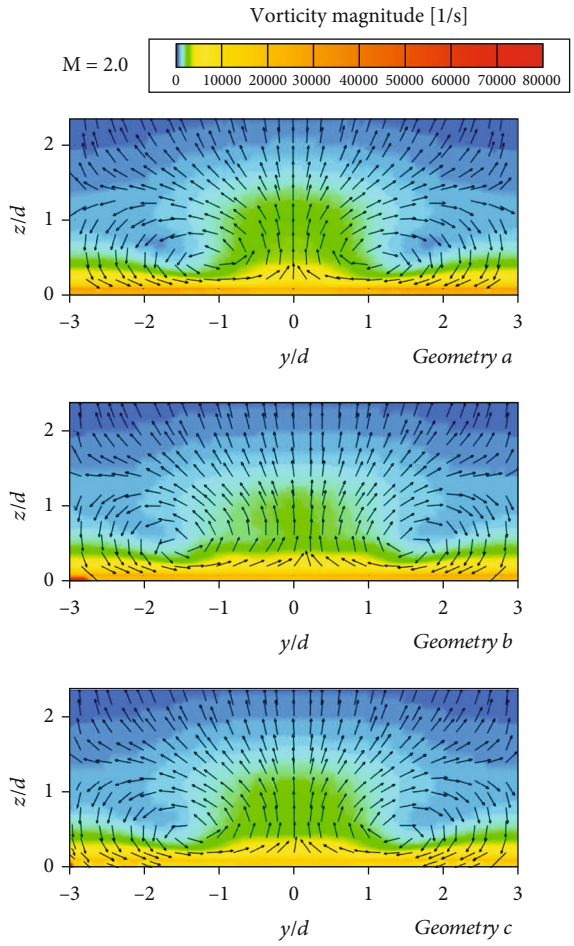

FIGURE 18: Vorticity magnitude contours and velocity vectors at x /d = 5, for the three film hole geometries, M = 2.

Figures 16–18 show the numerical contours of the vorticity magnitudes and velocity vectors on a plane normal to the main flow at x/d = 5. Kidney vortices are observed in all nine cases. However, for *Geometries b* and *c*, at the blowing ratio of 0.5, we notice that the velocity vectors at y/d = 0 are pointing downward indicating that the coolant is suppressed to the film coverage surface.

5. Conclusions

The film effectiveness performance of three new film hole geometries was investigated both experimentally and numerically. Pressure-sensitive paint technique was used in the experimental part while the numerical analyses were done using the Fluent™ solver along with the realizable *k*-ε turbulence model. Comparisons were made between the results of the three proposed geometries and those of the commonly used 7°-7°-7° diffusion hole. The major conclusions of this study were: (a) the proposed geometries performed superior to the 7°-7°-7° diffusion hole for the three tested blowing ratios of 0.5, 1, and 2, (b) the film effectiveness results for these three film holes, which had different expansion section geometries due to the manner by which the circular feed hole was blended into the expansion section, were not significantly different from each other indicating that manufacturing tolerances associated with the laser-drilling of the film hole exits may not have a significant effect on the overall film effectiveness performance, and (c) numerical results using the realizable *k*-ε turbulence model were in reasonable agreement with the test data.

Abbreviations

C: Chemical concentration [%]
D_h: Main channel hydraulic diameter [0.061 m]
d: Inlet hole diameter (Figure 4) [3.81 mm]
I: Light intensity (pixel intensity value)
IR: The ratio of reference light intensity and measured intensity
L: Total axial length of each film hole [22.86 mm]
ℓ: Feed (entrance) hole length (9.53 mm)
$\dot{m}_{N_2}$: Nitrogen flow rate in each tripod [kg/s]
$\dot{m}_{air}$: Main channel air mass flow rate [kg/s]
M: Blowing ratio, $(\dot{m}_{N_2}/(\pi d^2/4))/(\dot{m}_{air}/A_{passage})$
M_c: Coolant molecular weight [28 kg/kmol]
M_∞: Mainstream (air) molecular weight [28.97 kg/kmol]
p: Hole pitch [22.86 mm]
P: Pressure [Pa]
Pr: Prandtl number
PSP: Pressure sensitive paint
$P_{O_2,air}$: Oxygen partial pressure in main channel approach air [Equation (1), 21 kPa]
$P_{O_2,mix}$: Oxygen partial pressure at a given point downstream the film holes [Equation (1), kPa]
Re: Reynolds number based on the passage hydraulic diameter, $[(\rho U D_h/\mu) = 87200]$
T: Temperature
TSP: Temperature sensitive paint
U: Main passage air velocity [m/s]
α: Hole inclination angle, 30° (Figure 3)
β_1: Shaped hole laid-back angle (Figure 2)
β_2: Shaped hole lateral expansion angle (Figure 2)
η: Film cooling effectiveness
μ: Air dynamic viscosity [kg/(ms)]
ρ: Air density [kg/m^3].

Subscripts

aw: Adiabatic wall
blk: Black
c: Coolant
O_2: Diatomic oxygen
N_2: Nitrogen
ref: Reference
∞: Channel mainstream.

Data Availability

Data files are available upon request.

Conflicts of Interest

The authors declare that they have no conflicts of interest.

Funding

All internal funds.

References

[1] J. C. Han, "Turbine blade cooling studies at Texas A&M University: 1980-2004," *Journal of Thermophysics and Heat Transfer*, vol. 20, no. 2, pp. 161–187, 2006.

[2] C. F. McDonald, "Power conversion system considerations for a high efficiency small modular nuclear gas turbine combined cycle power plant concept (NGTCC)," *Applied Thermal Engineering*, vol. 73, no. 1, pp. 82–103, 2014.

[3] N. E. Kukharkin, N. N. Ponomarev-Stepnoi, and V. A. Usov, *Nuclear Power Sources for Space Systems, Handbook of Nuclear Chemistry*, Springer, US, 2011.

[4] D. G. Bogard and K. A. Thole, "Gas turbine film cooling," *Journal of Propulsion and Power*, vol. 22, no. 2, pp. 249–270, 2006.

[5] J. L. Kerrebrock, *Aircraft Engines and Gas Turbines*, MIT Press, Cambridge, Massachusetts, 2001.

[6] V. L. Eriksen and R. J. Goldstein, "Heat transfer and film cooling following normal injection through a round hole," *Journal of Engineering for Power*, vol. 96, no. 4, pp. 329–334, 1974.

[7] R. S. Bunker, "A review of shaped hole turbine film-cooling technology," *Journal of Heat Transfer*, vol. 127, no. 13, pp. 441–453, 2005.

[8] R. Krewinkel, "A review of gas turbine effusion cooling studies," *International Journal of Heat and Mass Transfer*, vol. 66, pp. 706–722, 2013.

[9] J. E. Hatch and S. S. Papell, *Use of a theoretical flow model to correlate data for film cooling on heating an adiabatic wall by tangential injection of gases of different fluid properties*, National Aeronautics and Space Administration, Technical Note D-130, 1959.

[10] R. J. Goldstein, "Film cooling," *Advances in Heat Transfer*, vol. 7, pp. 321–379, 1971.

[11] P. Ligrani, "Aerodynamic losses in turbines with and without film cooling, as influenced by mainstream turbulence, surface roughness, airfoil shape, and mach number," *International Journal of Rotating Machinery*, vol. 2012, Article ID 957421, 28 pages, 2012.

[12] C. R. B. Day, M. L. G. Oldfield, and G. D. Lock, "Aerodynamic performance of an annular cascade of film cooled nozzle guide vanes under engine representative conditions," *Experiments in Fluids*, vol. 29, no. 2, pp. 117–129, 2000.

[13] R. J. Goldstein, E. R. G. Eckert, and F. Burggraf, "Effects of Hole Geometry and Density on Three-Dimensional Film Cooling," *International Journal of Heat and Mass Transfer*, vol. 17, no. 5, pp. 595–607, 1974.

[14] B. Sen, D. L. Schmidt, and D. G. Bogard, "Film cooling with compound angle holes: heat transfer," in *Proceedings of the ASME 1994 International Gas Turbine and Aeroengine Congress and Exposition. Volume 4: Heat Transfer; Electric Power; Industrial and Cogeneration*, 8 pages, The Hague, Netherlands, 1994.

[15] D. L. Schmidt, B. Sen, and D. G. Bogard, "Film cooling with compound angle holes: adiabatic effectiveness," in *Proceedings of the ASME 1994 International Gas Turbine and Aeroengine Congress and Exposition. Volume 4: Heat Transfer; Electric Power; Industrial and Cogeneration*, 8 pages, The Hague, Netherlands, 1994.

[16] K. Thole, M. Gritsch, A. Schulz, and S. Wittig, "Flowfield measurements for film cooling holes with expanded exits," in *Proceedings of the ASME 1996 International Gas Turbine and Aeroengine Congress and Exhibition. Volume 4: Heat Transfer; Electric Power; Industrial and Cogeneration*, 10 pages, Birmingham, UK, 1996.

[17] A. Kohli and K. A. Thole, "Entrance effects on diffused film cooling holes," in *Proceedings of the ASME 1998 International Gas Turbine and Aeroengine Congress and Exhibition. Volume 4: Heat Transfer; Electric Power; Industrial and Cogeneration*, 8 pages, Stockholm, Sweden, 1998.

[18] M. Gritsch, A. Schulz, and S. Wittig, "Adiabatic wall effectiveness measurements of film-cooling holes with expanded exits," in *Proceedings of the ASME 1997 International Gas Turbine and Aeroengine Congress and Exhibition. Volume 3: Heat Transfer; Electric Power; Industrial and Cogeneration*, 10 pages, Orlando, Florida, USA, 1997.

[19] M. Gritsch, A. Schulz, and S. Wittig, "Heat transfer coefficients measurements of film-cooling holes with expanded exits," in *Proceedings of the ASME 1998 International Gas Turbine and Aeroengine Congress and Exhibition. Volume 4: Heat Transfer; Electric Power; Industrial and Cogeneration*, 11 pages, Stockholm, Sweden, 1998.

[20] Y. Yu, C.-H. Yen, T. I.-P. Shih, M. K. Chyu, and S. Gogineni, "Film cooling effectiveness and heat transfer coefficient distributions around diffusion shaped holes," in *Proceedings of the ASME 1999 International Gas Turbine and Aeroengine Congress and Exhibition. Volume 3: Heat Transfer; Electric Power; Industrial and Cogeneration*, 11 pages, Indianapolis, Indiana, USA, 1999.

[21] A. Kohli and D. G. Bogard, "Effects of hole shape on film cooling with large angle injection," in *Proceedings of the ASME 1999 International Gas Turbine and Aeroengine Congress and Exhibition. Volume 3: Heat Transfer; Electric Power; Industrial and Cogeneration*, 7 pages, Indianapolis, Indiana, USA, 1999.

[22] D. J. Jackson, K. L. Lee, P. M. Ligrani, P. D. Johnson, and F. O. Soechting, "Transonic aerodynamic losses due to turbine airfoil suction surface film cooling," in *Proceedings of the ASME 1999 International Gas Turbine and Aeroengine Congress and Exhibition. Volume 3: Heat Transfer; Electric Power; Industrial and Cogeneration*, 11 pages, Indianapolis, Indiana, USA, 1999.

[23] C. Saumweber, A. Schulz, S. Wittig, and M. Gritsch, "Effects of entrance cross-flow directions to film cooling holes," *Annals of the New York Academy of Sciences*, vol. 934, no. 1, pp. 401–408, 2001.

[24] R. P. Schroeder and K. A. Thole, "Adiabatic effectiveness measurements for a baseline shaped film cooling hole," in *Proceedings of the ASME Turbo Expo 2014: Turbine Technical Conference and Exposition. Volume 5B: Heat Transfer*, 13 pages, Düsseldorf, Germany, 2014.

[25] S. Haydt, S. Lynch, and S. Lewis, "The effect of area ratio change via increased hole length for shaped film cooling holes with constant expansion angles," *Journal of Turbomachinery*, vol. 140, 13 pages, 2018.

[26] X. Sun, G. Zhao, P. Jiang, W. Peng, and J. Wang, "Influence of hole geometry on film cooling effectiveness for a constant exit flow area," *Applied Thermal Engineering*, vol. 130, no. 5, pp. 1404–1415, 2018.

[27] T. B. Watson, K. R. Vinton, L. M. Wright, D. C. Crites, M. C. Morris, and A. Riahi, "Influence of hole inlet geometry on the film cooling effectiveness from shaped film cooling holes," in *Proceedings of the ASME Turbo Expo 2019: Turbomachinery*

Technical Conference and Exposition. Volume 5B: Heat Transfer, 10 pages, Phoenix, Arizona, USA, 2019.

[28] D. Charbonnier, P. Ott, M. Jonsson, F. Cottier, and T. Kobke, "Experimental and numerical study of the thermal performance of a film cooled turbine platform," in *Proceedings of the ASME Turbo Expo 2009: Power for Land, Sea, and Air. Volume 3: Heat Transfer, Parts A and B*, 12 pages, Orlando, Florida, USA, 2009.

[29] J. Kavandi, J. Callis, M. Gouterman et al., "Luminescent barometry in wind tunnels," *Review of Scientific Instruments*, vol. 61, no. 11, pp. 3340–3347, 1990.

[30] J. W. Gregory, K. Asai, M. Kameda, T. Liu, and J. P. Sullivan, "A review of pressure-sensitive paint for high-speed and unsteady aerodynamics," *Journal of Aerospace Engineering*, vol. 222, no. 2, pp. 249–290, 2008.

[31] F. Baldino and M. E. Taslim, "Experimental film cooling effectiveness of multi-row patterns on flat and step-down surfaces," in *Proceedings of the ASME Turbo Expo 2019: Turbomachinery Technical Conference and Exposition. Volume 5B: Heat Transfer*, 16 pages, Phoenix, Arizona, USA, 2019.

[32] S. J. Kline and F. A. McClintock, "Describing uncertainty in single-sample experiments," *Mechanical Engineering*, vol. 75, pp. 3–8, 1953.